Energy Storage Materials 69 (2024) 103414

Contents lists available at ScienceDirect

Energy Storage Materials

journal homepage: www.elsevier.com/locate/ensm

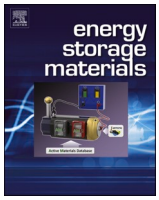

Understanding charge transfer dynamics in blended positive electrodes for Li-ion batteries

Dimitrios Chatzogiannakis [a,b,c], Violetta Arszelewska [d], Pierre-Etienne Cabelguen [d], François Fauth [e], Montse Casas-Cabanas [a,f,*], M. Rosa Palacin [b,**]

[a] Centro de Investigación Cooperativa de Energías Alternativas (CIC energiGUNE), Basque Research and Technology Alliance (BRTA), Vitoria-Gasteiz 01510, Spain
[b] Institut de Ciència de Materials de Barcelona, ICMAB-CSIC, Campus UAB, Bellaterra, Catalonia 08193, Spain
[c] ALISTORE-ERI, CNRS FR 3104, France
[d] UMICORE, 31 rue du Marais, Brussels 1000, Belgium
[e] CELLS-ALBA Synchrotron, Cerdanyola del Vallès, Barcelona 08290, Spain
[f] Ikerbasque - Basque Foundation for Science, Maria Diaz de Haro 3, Bilbao 48013, Spain

ARTICLE INFO

Keywords:
Blended electrodes
Operando XRD
Cathode materials
Li-ion
Beam effects
Electrode dynamics

ABSTRACT

This paper investigates the electrochemical behavior of binary blend electrodes comprising equivalent amounts of lithium-ion battery active materials, namely $LiNi_{0.5}Mn_{0.3}Co_{0.2}O_2$ (NMC), $LiMn_2O_4$ (LMO), $LiFe_{0.35}Mn_{0.65}PO_4$ (LFMP) and $LiFePO_4$ (LFP)), with a focus on decoupled electrochemical testing and *operando* X-ray diffraction (XRD). All possible 50:50 blend combinations were studied and the distribution of current between blend components was followed during continuous and pulsed charge and discharge processes. The results demonstrate the significant impact of the voltage profiles of individual materials on the current distribution, with the effective C-rate of each component varying throughout the State of Charge (SoC). Pulsed decoupled electrochemical testing reveals the exchange of charge between blend components during relaxation, showcasing the "buffer effect", which has also been captured through time-resolved *operando* XRD experiments in real blends carefully considering beam-induced effects. The directionality and magnitude of the charge transfer were found to depend on the nature of the components and the cell SoC, being also influenced by temperature. These dependencies can be rationalized considering both thermodynamics (voltage profile) and reaction kinetics of the blend constituents. These findings contribute to advancing the understanding of internal dynamics in blended electrodes, offering valuable insights for the rational design of blends to meet the diverse operational demands of lithium-ion batteries.

1. Introduction

Transport electrification has resulted in an expansion of the Li-ion battery market from its original scope embracing mostly portable electronics. This has brought up challenges in terms of scale (from Wh to kWh storage) which involve not only building larger cells but also their assembly in modules and packs. These are controlled by a Battery Management System (BMS) to ensure safe and reliable operation while also mitigating performance loss as much as possible. Aside improvements in cell size and cycle life, additional battery requirements brought up by the advent of electric vehicles are related to performance indicators (e.g. in terms of power), enhancement of sustainability and decrease of cost.

Blending different active materials in the same cell electrode, an empirical approach commonly used for primary cells has been readily applied to commercial EV Li-ion batteries, mostly on the positive side [1], despite unfortunately receiving rather low attention at the fundamental research level. The global aim is to promote positive synergetic effects between the different electrode components (typically $LiMn_2O_4$ and layered $LiMO_2$ with M consisting of Ni, Co and Mn or Al). Several different strategies have been identified to achieve this goal.

On the chemical side, and as pointed out by Numata *et al.* (NEC

* Corresponding author at: Centro de Investigación Cooperativa de Energías Alternativas (CIC energiGUNE), Basque Research and Technology Alliance (BRTA), Vitoria-Gasteiz 01510, Spain.
** Corresponding author.
E-mail addresses: mcasas@cicenergigune.com (M. Casas-Cabanas), rosa.palacin@icmab.es (M.R. Palacin).

https://doi.org/10.1016/j.ensm.2024.103414
Received 31 January 2024; Received in revised form 12 April 2024; Accepted 16 April 2024
Available online 17 April 2024

corporation) more than 20 years ago [2], the capacity fade in $LiMn_2O_4$ caused by manganese dissolution related to acid leaching could be alleviated by blending with $LiMO_2$. The underlying rationale behind is that the basicity of $LiMO_2$ would help in mitigating the presence of hydrofluoric acid (HF) in the electrolyte, which can result from hydrolysis of PF_6^- anions present in the electrolyte caused by H_2O impurities. In addition to that, the presence of $LiMn_2O_4$ would contribute to decrease the total amount of cobalt in $LiMO_2$ electrodes, hence improving both battery cost and environmental footprint. Such compound specific features, which also involve the electrolyte and were also confirmed by later studies [3–6], exert an influence on thermal behaviour, consequently also impacting safety [6–8].

More generic aspects to be considered are particle sizes and reaction kinetics of the electrode active materials. Improvement in terms of loading density of the casted electrodes can result from tuning the electrode microstructure [9]. One notable example is mixing materials with different particle sizes (not necessarily involving different compositions), a practice that may be common at the industrial level despite it has not been extensively addressed in the scientific literature.

A few studies related to thermodynamics have been carried out [10–14] providing insights into the influence of temperature on the behaviour of the blended electrodes. Reversible heat generation rates are consistent with predictions based on the composition and properties of constituents. Yet, and as a result of the different entropy coefficients of the blend components, temperature changes will induce an internal charge transfer process (i.e. lithium exchange) which will take place even when batteries are at rest, for instance, while vehicles are parked.

Kinetic aspects are considered most relevant for practical application, and their rationalization would help in the design of blended electrodes optimized for operation under specific conditions. Materials with fast reaction kinetics can sustain significantly higher effective rates than the nominal rate applied to the electrode, which is beneficial for applications involving high pulse-like loads such as electric vehicles. Once the pulse is finished, relaxation will induce a redistribution of lithium within the components to reach equilibrium. This rationale has motivated the widespread commercial use of $LiMO_2$: $LiMn_2O_4$ blends. $LiMO_2$, despite having slow kinetics, exhibits high capacity (especially for large amounts of *M*=Ni). The addition of $LiMn_2O_4$ lowers overall costs while enhancing power performance. Olivine $LiMPO_4$ (*M*=Fe, Mn) based blends have a lower presence in commercial cells to date but they have also deserved attention at the laboratory scale as they can as well exhibit fast kinetics and are based on low cost abundant transition metals (See [15] as an example together with general review papers [16, 17]).

The study of interactions rooted in different kinetics (improvement of electrode rate capability sometimes referred to as “buffer effect”) has significantly progressed in recent years thanks to the approach developed by Heubner *et al.*, adapted from corrosion studies, which enables to separate the current responses from the individual blend components using three electrode cells. [13,18,19]. By using an analogous setup for the study of $LiMn_2O_4$: $LiNi_{0.5}Mn_{0.3}Co_{0.2}O_2$ blends [17], the effective current load on each blend component was found to be very different depending on SoC and ratio of blended components. This finding was in full agreement with results from *operando* synchrotron X-ray absorption and diffraction experiments carried out on real blend electrodes where the components are in physical contact [20].

The present paper aims to broaden the scope by including a wider set of blends, with every binary 50:50 combination of $LiMn_2O_4$ (LMO), $LiNi_{0.5}Mn_{0.3}Co_{0.2}O_2$ (NMC), $LiFePO_4$ (LFP) and $LiFe_{0.35}Mn_{0.65}PO_4$ (LFMP), well known materials applied in commercial cells and exhibiting not only different kinetics but also different voltage profiles. The above mentioned three electrode cell setup was also used, for both continuous and pulsed galvanostatic experiments, and coupled to time-resolved synchrotron *operando* X-ray diffraction experiments, to capture and rationalize charge transfer events between blend components as a function of thermodynamical (voltage profile) and reaction kinetics of individual blend components.

2. Experimental details

2.1. Decoupled blend study

In order to investigate the effective current loads experienced by each blend component (as opposed to the nominal applied rate) and the amount of charge exchanged during the relaxation steps, the decoupled blend setup developed by Heubner *et al.* was used [13]. This setup, which allows mimicking the electrochemical response of a blended electrode while monitoring individual current contributions, is comprised of a three electrode Swagelok cell (perfluoroalkoxyalcane (PFA) body) with two positive working electrodes (each containing one of the blend components) and a third common negative lithium metal counter electrode.

The electrode formulation used consists of 84:8:8 (Active material (Pure or blended): Super P (Thermo Scientific): PVDF (Kureha). $LiMn_2O_4$ (LMO) was purchased from Sigma Aldrich, $LiNi_{0.5}Mn_{0.3}Co_{0.2}O_2$ (NMC) from MTI corp., and $LiFePO_4$ (LFP) and $LiFe_{0.35}Mn_{0.65}PO_4$ (LFMP) from Aleees. N-Methyl-2-Pyrrolidone (NMP)-based slurries were tape casted (250 μm) onto aluminum foil (SAMA), dried at 120 °C, and punched into 14 mm discs, calendared at 4 Tons and later further punched to reduce the diameter to 10 mm before a final drying at 120 °C under vacuum overnight. The electrodes were then transferred to a glovebox (Argon-filled, $H_2O < 0.5$ ppm, $O_2 < 2$ ppm) for assembly, ensuring minimal exposure to ambient humidity or oxygen throughout the entire process.

For each cell, two electrodes of the same diameter (10 mm) and areal loading (4–5 mg/cm^2) were selected trying to achieve an active mass ratio as close to 50:50 as possible. The achieved ratios, capacities and 1C specific currents are listed in Table 1 S.I. The cells were first cycled 3 times at a rate of C/10 in the 4.3-3.2 V range, including 1 h long constant voltage steps at the upper and lower cutoff voltages, while recording the current flowing to/from each of the two working electrodes. After a final charge (and 1 h constant voltage step) at C/10 up to 4.3 V, the cells were discharged through 20 pulses at a rate of 3C, each lasting 1 min. After each pulse, the cell underwent a 10 min relaxation period in OCV (Open Circuit Voltage), with the current flowing between the electrodes containing the individual blend components being measured both during the pulse and the relaxation. To have a consistent protocol for all the blends, no lower cutoff voltage was used. Before this measurement, no cell had been discharged at voltages lower than 3.2 V.

For the measurements done at 40 °C, a recirculating bath (Thermo Scientific) filled with silicon oil was used. After it reached the target temperature, individual zip bags containing the 3 electrode cells, were immersed in the oil where they were left for at least 24 h to thermalize. Afterwards, the same protocols used at room temperature were applied.

2.2. Synchrotron X-Ray diffraction

High resolution XRD measurements were carried out at BL-04 (MSPD) beamline of ALBA synchrotron in transmission geometry using a MYTHEN2 high-throughput position sensitive detector. The cells used were specially adapted Hohsen CR2032 coin cells [21] (Institute for Applied Materials - Energy Storage Systems Karlsruhe Institute of Technology), bearing a thin glass window on both sides and a hole on the stainless-steel spacer, but otherwise identical to the standard CR2032 ones. Glass windows (130 μm thick) were selected because of their rigidity and a Kapton disc was placed on the hole of the current collector/spacer [22]. Both contribute to achieving a more homogeneous cell pressure, critical in such experiments at fast rates. The cells were mounted on an 8 coin cell carousel-like holder enabling sequential data acquisition [21] and cycled using a VSP potentiostat-galvanostat (Bio-Logic). The electrodes used in the experiments, each one containing a 50:50 blend, were prepared using the same techniques and

materials described in Section 2.1 and treated in the same way differing only in their diameter which was in this case was kept at 14 mm. Their capacities and 1C specific currents are given in Table 2 S.I.

Since beam effects during *operando* experiments have been previously reported [23–26] precautions were taken to optimize the data acquisition protocol and experiments were done at two different photon energies 15 keV (λ = 0.8265 Å) and 30 keV (λ = 0.4135 Å). Before being mounted on the beamline cell holder, all cells were pre-charged slowly (C/10 for pulsed and C/5 for continuous testing) up to 4.3 V and then kept at constant voltage (CV) for at least 1 h. During continuous discharges, cells were cycled in parallel while sequentially exposed to the beam to acquirediffraction patterns. This protocol resulted in approximately 6 min intervals between two successive paterns on each cell, thus avoiding continuous irradiation. For the pulsed experiments, a protocol comparable to the one used in the decoupled blend study was used, with 20, 1 min long, 3C discharge pulses. After each 1 min discharge pulse and 10 min relaxation (11 min of total beam exposure), the cell was left without irradiation for approx. 1 h to allow for the recovery of any possible reversible beam-induced effects. The area where the relaxations were recorded remained unirradiated during the pulse and was only exposed to the beam (3 × 1 mm) after the current cutoff. During the 10 min acquisition the cell was oscillated ±1 mm to create an effective exposed area of approximately 3 × 3 mm, thereby reducing the accumulated radiation dose per unit area of the electrode.

3. Results and discussion

3.1. Decoupled blend continuous electrochemical testing

The 4 materials under study, $LiNi_{0.5}Mn_{0.3}Co_{0.2}O_2$ (NMC), $LiMn_2O_4$ (LMO), $LiFe_{0.35}Mn_{0.65}PO_4$ (LFMP) and $LiFePO_4$ (LFP), were initially measured in the decoupled setup, simulating the 6 possible two component blend combinations: NMC-LFP, NMC-LMO, NMC-LFMP, LFP-LFMP, LMO-LFMP and LMO-LFP. The individual components differ significantly in their voltage vs capacity profiles (see Fig. 1S.I.) which are sloping for NMC, single plateau for LFP, two plateaus at very close potentials for LMO and two plateaus at significantly different potentials for LFMP.

Fig. 1 depicts the voltage (in blue) as a function of time for the last C/10 cycle of all the cells. The solid black line indicates the current flowing exclusively to one of the materials (determined by the cell's connection), while the dashed black line indicates the total (dis)charging current of the cell distributed between the two materials. The shaded areas indicate the amount of charge stored or provided by each one of them. Colour coding has been implemented throughout this article with NMC marked in Green, LFMP in Black, LFP in Red and LMO in Blue. Voltage vs capacity curves for all the cells can be found in Fig. 2S.I.

The distribution of the current between the two blend components depends on the individual voltage profile of the materials, and therefore varies significantly with the SoC. Except for the case of NMC-LMO, each component's contribution ranges from ca. 0 % to ca. 100 % throughout both charge and discharge, which is related to the little overlap between the voltage profiles of the two materials.

Since each material accounts for 50 % of the active mass of the blend, and the cell's nominal C-rate is calculated taking into account the total expected capacity, the effective C-rate for a component in the areas where it has 100 % contribution will be substantially higher (exactly double if both materials had the same capacity). This situation contrasts with the case of an electrode containing a single active material, which would withstand a constant C-rate throughout the full voltage range. Blended electrodes exhibit thus an extra level of complexity because the effective rate can significantly vary depending on the cell SoC. Since lithium intercalation kinetics in active materials may also depend on their level of lithiation, blends could be designed to reduce the load of a specific component during a "low kinetics" region and increase it for the "fast kinetics" phase, tailoring them to the real application operation conditions (e.g. voltage window and power). Furthermore, the magnitude of this load increase/decrease could also be modified by changing the mass ratio between the blend components, though this remains out of the scope of this study.

The results depicted in Fig. 1 clearly indicate that the distribution of current for the charge and discharge processes is rather symmetrical, which indicates reversibility of the processes taking place regardless the direction of the current. The minor differences observed in some cases are attributed to overpotential and depend on the cell rate and the kinetics of the materials. The latter may vary with the SoC resulting in

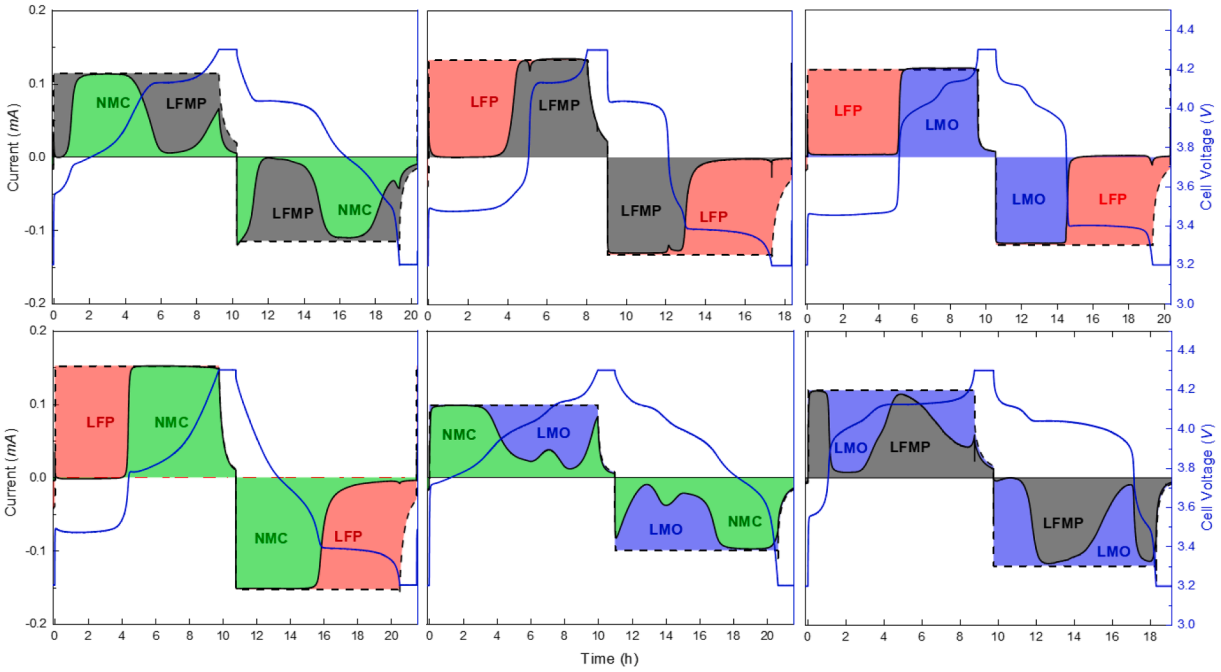

Fig. 1. Voltage profiles (Blue Lines) and charge distribution (shaded areas) in each of the 6 combinations of the selected materials when tested using the decoupled blend setup. The dashed black line shows the total (dis)charging current of the cell, set to achieve a cell nominal rate of C/10.

different overpotentials during lithiation or delithiation.

Interestingly, blends containing LFP exhibit a stepwise change in current contribution when the voltage of the blend is close to 3.4 V, the value at which the potential vs capacity profile of LFP exhibits a very flat plateau (Fig. 1S.I.). During charge, the activity of LFP is initially 100 % but falls to near 0 % when the blend voltage exceeds the LFP plateau voltage. A similar situation occurs with LFMP. However, since the characteristic curve of this material exhibits two plateaus at around 3.5 V and 4.05 V (Fig. 1S.I.), the activity of LFMP distinctly rises twice during both charge and discharge for both LFMP-LMO and LFMP-NMC, which is when the voltage of the blend coincides with the voltage corresponding to the plateaus. Since NMC exhibits a sloping voltage vs capacity profile, its contribution in a blend with a material exhibiting plateaus tends to increase when the voltage of the cell is above, below or in between the plateaus of the other material. Conversely, the contribution of NMC decreases dramatically when the cell voltage coincides with the plateau voltage of the other material.

This phenomenon can also be explained in terms of the rate of change of charge with respect to voltage, expressed as dQ/dV. The sloping behaviour of NMC results in a significant dQ/dV value throughout its working voltage range, while the other materials display a spike in dQ/dV at their voltage plateau and reach values close to 0 at the other voltages. The material with the higher contribution at each blend cell operation voltage is the one with higher dQ/dV. This is showcased in Fig. 2 for the case of NMC-LMO where dQ/dV measured for a C/10 discharge of two coin cells containing electrodes with only NMC (Green) or only LMO (Red) as active materials are plotted together with the current going to NMC in the NMC-LMO decoupled blend experiment (Black dashed line), also carried out at C/10. These results demonstrate a close agreement between the results of both types of experiments, as the current directed to NMC closely aligns with the total cell current (solid black line) when LMO's dQ/dV is close to 0. This is evident at voltages higher than 4.2 V or lower than 3.9 V. In contrast, at 4.12 V and 4.00 V, where plateaus of LMO are observed, NMC current drops to very low values (indicating that LMO's current is very high). In the region around 4.1 V, where the two materials have similar dQ/dV values, the current is shared between them, in agreement with the expectations. As the discharge C-rate increases, the dQ/dV peaks are expected to shift towards lower voltages according to the rate each material is experiencing and its reaction kinetics. For a continuous discharge and electrodes containing a single active materials this rate will be constant yet in blended electrodes this peak shift will be more complex due to the non-constant rate, and different for each of the blended active materials.

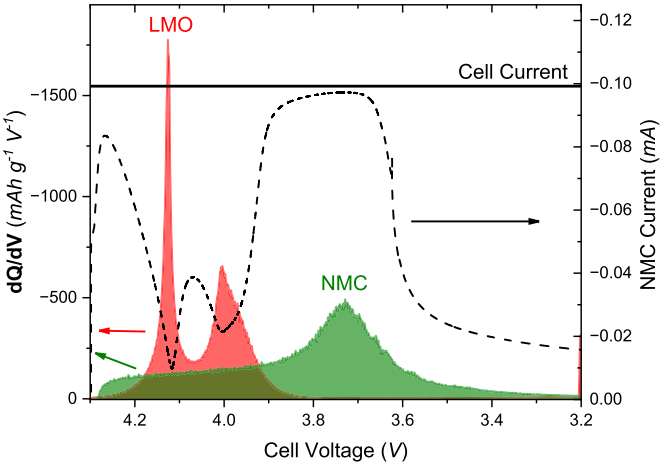

Fig. 2. dQ/dV of NMC (Green) and LMO (Red) as measured from coin cells of the pure materials and NMC's current (Black dashed line) during the decoupled NMC-LMO blend experiment. Solid black line shows the total discharge current of the decoupled blend cell.

With sufficient knowledge of the reaction kinetics and the material specific rates, dQ/dV plots could potentially be used as a prognostic tool for blended electrodes.

3.2. Decoupled blend pulsed electrochemical testing

Galvanostatic discharge pulses were also applied to the decoupled blends in order to monitor the exchange of charge between blend components during relaxation on the same cells used previously for the continuous charge/discharge protocol. as described in Section 2.1.

Fig. 3a illustrates the pulsed discharge data obtained for the NMC-LMO blend while those corresponding to the rest of combinations can be found in Fig. 4S.I. The top figure shows the evolution of cell voltage vs time during the pulsed discharge, while the bottom plot represents the NMC current vs time. The latter reveals that current of significant magnitude flows between blend components during relaxation as indicated by the shaded areas. This current is represented in different colours depending on its direction, where green shows the current from LMO to NMC and red from NMC to LMO, as schematically shown in Fig. 3b for three representative pulses.

During a high current pulse and due to the high flux of lithium towards one of the components causing a growing overpotential, it may become favorable for the lithium to be incorporated into the other material (depending on its voltage profile). Since this is an out of equilibrium condition, when the flux of lithium (cell current) is cut and the overpotential diminishes, lithium ions will be transferred between components to reach equilibrium. This phenomenon has been studied before, and is commonly referred to as the "buffer effect". However the studies presented herein allow to infer that the directionality of this current can vary with voltage (and therefore, with cell SoC), which is rooted both in thermodynamic aspects (voltage profile) and individual reaction kinetics, which in turn may vary with SoC for each component. In this case LMO accommodates excess lithium during the first galvanostatic discharge pulse and beyond pulse number 10. Hence during the relaxation period, lithium will be transferred from LMO to NMC. The situation is however reversed during pulses 2–10, where NMC is able to accommodate excess lithium during the pulse, and LMO accepts the extra lithium during relaxation.

Fig. 4 shows the magnitude and directionality of the relaxation current observed for each of the four materials when blended with any of the other three. This is presented as a function of the specific capacity of the blend specifying which material acts as a lithium donor (positive y values) or lithium acceptor (negative y values) during the pulse relaxation. Building upon the example of LMO—NMC outlined earlier, the top-left graph reveals that, except for the first pulse, NMC serves as a Li^+ donor until pulse 12 and transitions to an acceptor role from pulse 12 onward. This behaviour is analogous to what happens when blended with LFMP. In contrast, when blended with LFP, NMC predominantly operates as a Li^+ acceptor.

3.3. Effect of temperature in the relaxation current

The above results allow to assess the variation of the magnitude and the directionality of the current exchange between blend components, which is dictated by the voltage profiles of the active materials. Yet, other factors are expected to play an additional role, such as the relative particle sizes, electrode formulation and properties as well as temperature, that directly affects kinetics, the extent of the effect being also different depending on SoC.

To explore the effect of temperature, a new set of identical cells was made, and the same electrochemical protocol described in 3.1 was applied to them after they were thermalized at 40 °C. Fig. 5a shows the comparison of the measurements done for blends of NMC at 25 °C and 40 °C. First, with increasing temperature, the relaxation specific current peaks at higher values, which could be explained by the enhanced conductivity of the electrolyte as well as the faster kinetics of lithium

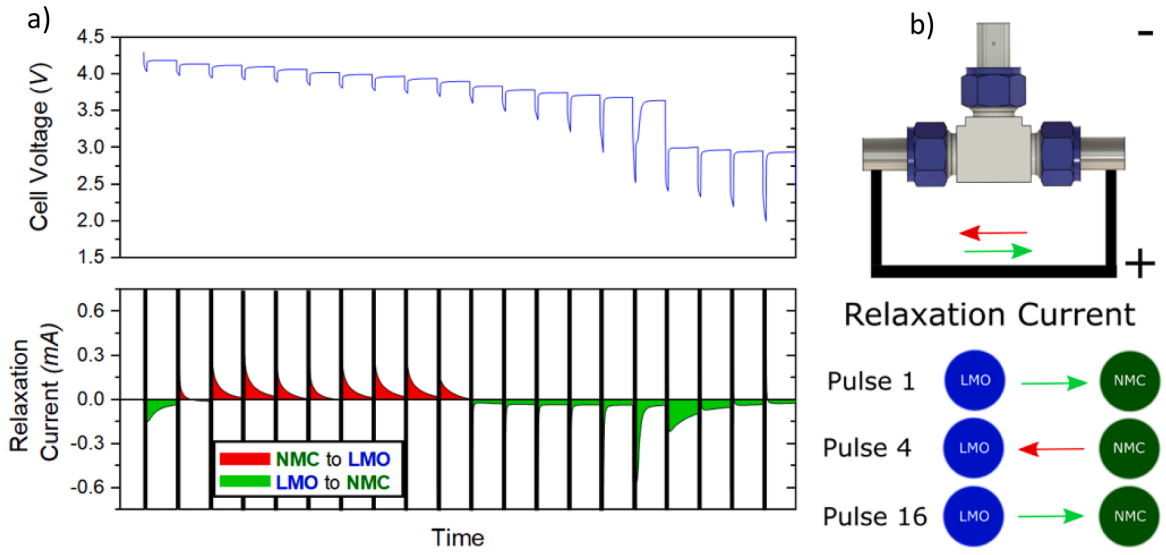

Fig. 3. (a) Pulsed discharge protocol showing the voltage vs time (top) as well as the relaxation current (bottom), color coded depending on the lithium flow direction (green for LMO to NMC and red for NMC to LMO). (b) Graphical representation of the cell and the relaxation current (top), direction of the relaxation current for selected pulses (bottom) of the present measurement.

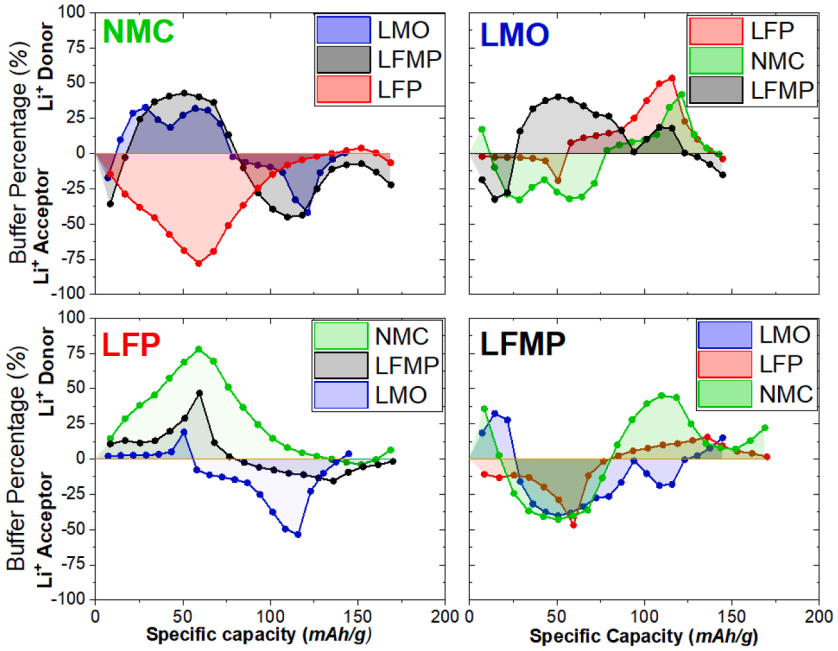

Fig. 4. Combined view of the charge transferred during relaxation (expressed as percentage of the total pulse charge) as a function of specific capacity for all the possible combinations of the 4 materials studied. The blends represented in each plot share one common component (written in the upper left corner of each plot) and the y-values indicate if this component acts as lithium donor (positive) or acceptor (negative) during post-pulse relaxation.

within the materials and at the material-electrolyte interfaces. However, at higher temperature, the total amount of charge exchanged between the materials during relaxation seems to have decreased. In Fig. 5b the value of the voltage after the 10 min relaxation, as well as the lowest voltage value recorded during the pulse, are depicted. It can be seen that, even though the relaxation voltages almost coincide for the two temperatures under study, there are significant discrepancies in the minimum voltage values recorded, which are systematically lower at 25 °C. The decrease of the overpotential for higher temperatures is something well established, yet what is deduced here is that the overpotential on each material is what drives the post-pulse inter-material relaxation. Increasing the overpotential is thus expected to also increase the amount of lithium transferred between blend components during relaxation, as shown in Fig. 5c.

An interesting case is that of pulses 3–9 for NMC-LFMP where the amount of lithium transferred during relaxation is higher at 40 °C. This is attributed to the fact that relaxation is not finished between two consecutive pulses (i.e. the current is still significant). It is expected that, given enough time to fully relax (with current approaching zero) the amount of charge transferred at high temperatures will be lower, as observed for the experiments involving blends containing LFP, LMO and NMC. This effect is however of interest, as pulsing an already out of equilibrium blended electrode could be a plausible scenario for batteries in real world situations as fast consecutive accelerations in electric vehicles.

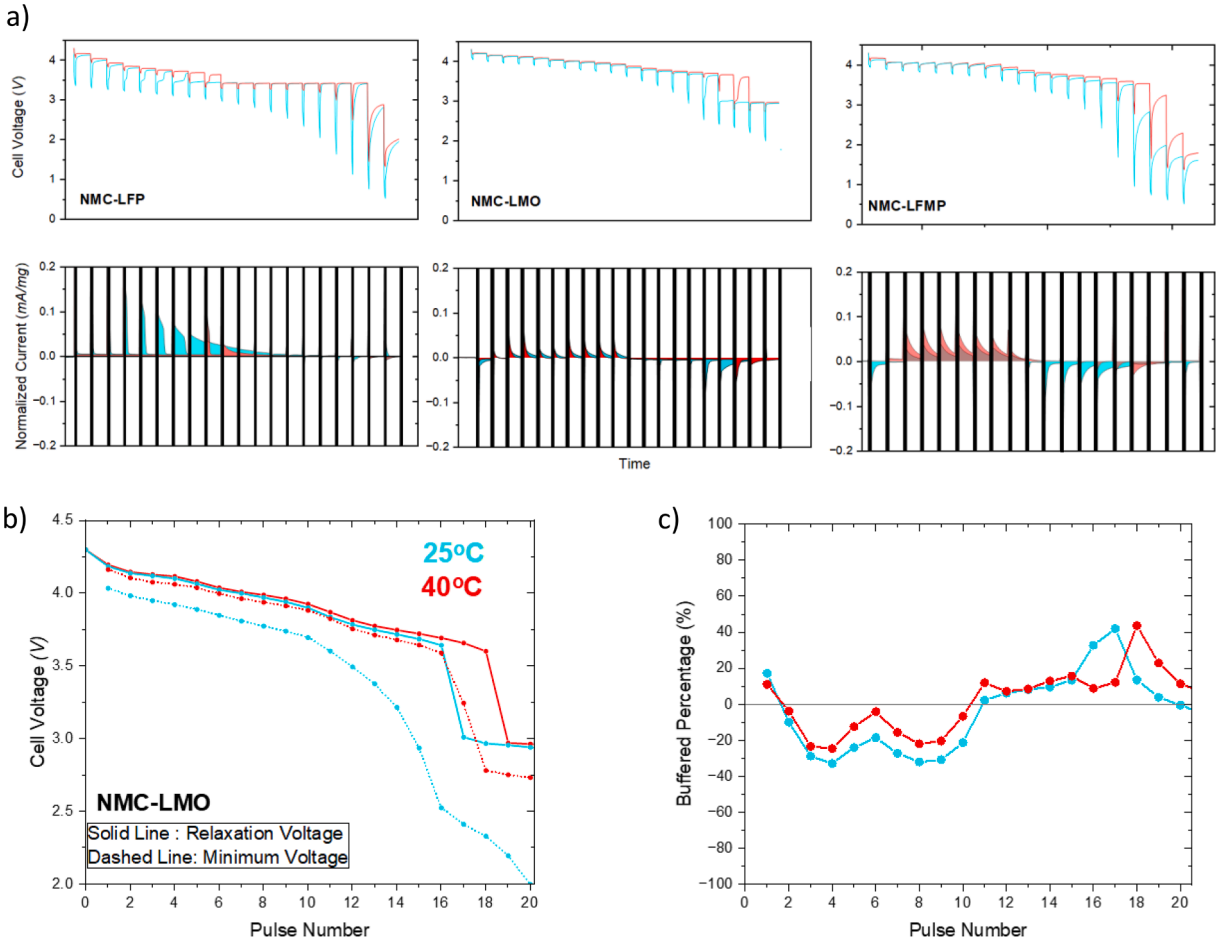

Fig. 5. (a) Comparison between pulsed discharges and relaxation currents at 25 °C and 40 °C (b) After relaxation and minimum voltages recorded for NMC-LMO blend at 25 °C and 40 °C (c) The relaxation charged expressed as the percentage of the total pulse charge.

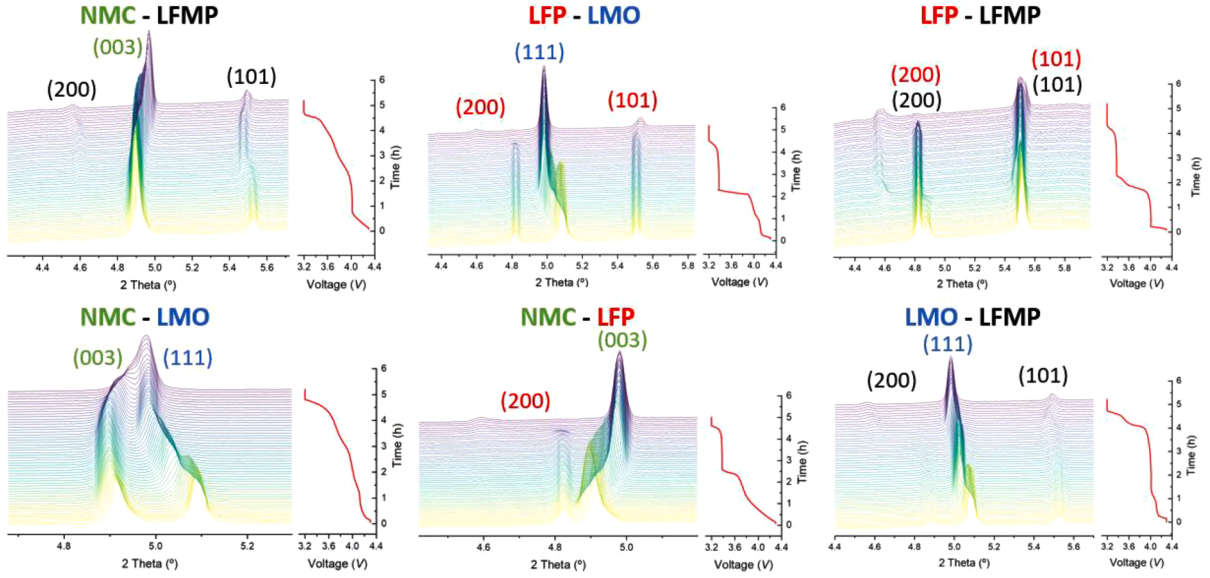

Fig. 6. Diffraction patterns recorded during continuous C/5 discharge of the blended electrodes at 30 keV ($\lambda = 0.4135$ Å) together with the corresponding voltage profile. Angular ranges depicted contain the more relevant and intense peaks of the blend components. Their Miller indices, colour coded according to material, are also shown.

3.4. Study of the internal dynamics in a blended positive electrode through operando X-Ray diffraction (XRD)

Operando X-ray diffraction was conducted as described in Section 2.2 to capture structural changes associated to charge transfer events between blend components through time-resolved experiments. In this case the blend components are not separated as in the decoupled blend study but physically mixed and part of a single electrode, providing complementary information. Initially, a low rate (C/5) continuous discharge was recorded for all the blends in the 4.3–3.2 V range to follow the evolution of the diffraction peaks. Fig. 6 below shows selected regions of the recorded patterns which enable to follow the evolution of specific peaks characteristic of each material as a function of SoC. The measured capacity vs voltage curves are shown in Fig. 3S.I. and show remarkable similarity with the curves measured for the decoupled blends regardless of the very different measurement setup and higher rate (C/5 for XRD and C/10 for the decoupled blends).

For NMC (R-3 m space group), there is a non-monotonic shift of the $(003)_{NMC}$ peak (initially at 4.9°) towards lower angles first, and in the opposite direction afterwards, in agreement with the expected behavior and well-known evolution of material's interlayer distance. For LMO spinel (Fd-3 m space group), the $(111)_{LMO}$ peak appears initially at 5.1° and shifts to lower angles upon lithium intercalation, again in good agreement with the expected behavior. Note that $(003)_{NMC}$ and $(111)_{LMO}$ reflections converge at the end of discharge. The $(200)_{FP}$ peak of the olivine $FePO_4$ (Pnma space group) appears at approx. 4.81° and decreases gradually in intensity (in agreement with the redox mechanism of LFP involving a first order phase transition) at the expense of the $(200)_{LFP}$ peak appearing at around 4.6°. The $(101)_{FP}$ peak is also seen at around 5.5° which slightly shifts to higher angles when lithiated. Finally, for the also olivine LFMP (Pnma space group) two peaks are observed, at 4.88° (200) and 5.52° (101). The low angle peak disappears while a peak rises at around 4.6° while the one at 5.52° shifts to lower angles until 5.48 ° and then again slightly towards higher angles. The behaviour of the observed peaks are in line with what is expected from their reaction mechanism.

Consistent with the results of the decoupled blend study (Fig. 1) the SoC of a specific active material, monitored through the evolution of its diffraction peaks, will evolve differently with the depth of discharge for each blend in which it is present. A good example is that of LMO when blended with LFP or LFMP. Due to the lower voltage of LFP compared to the significantly higher voltage of LMO, the two materials discharge sequentially withLMO undergoing full lithiation before lithium is inserted into LFP. This is demonstrated by the $(111)_{LMO}$ peak in the LFP-LMO blend in Fig. 6, which has reached its lithiated position after approximately 2.5 h and remains unchanged while LFP is active. Conversely, the behavior of LMO-LFMP blend is different, since LFMP is also active at high voltages, resulting in a more simultaneous discharge of the two materials. Once again, this can be showcased by the $(111)_{LMO}$ peak which in this case reaches its final position at the end of the discharge, and it is witnessed to evolve throughout the whole discharging process. A similar analysis can be applied to the NMC-LMO and the NMC-LFP blend. Focusing on the $(003)_{NMC}$ peak, when blended with LMO, much of the peak shift happens towards the end of discharge, after 3 h, which is in line with the decoupled blend study shown in Fig. 1 where NMC is predominantly active towards the end of the discharge. This phenomenon is reversed when NMC is combined with LFP, as both XRD and decoupled blends show NMC activity towards the beginning of the discharge. In this case, and similarly to the LMO-LFP blend, the materials discharge in a sequential fashion and as such the $(003)_{NMC}$ peak makes its full range of shift in the first half of the discharge.

Pulsed discharges including relaxation steps between consecutive pulses were also followed by *operando* XRD. While voltage profiles and the directionality of lithium during relaxation are expected to be similar to those observed in the experiment using the decoupled blend setup described in Section 3.2, we anticipate slight differences in kinetics due to the faster lithium exchange in a true blended cathode where the components are in direct contact.

As described in Section 2.2, the *operando* experiments to follow both pulses and relaxation between successive pulses were carried out at both 15 keV and 30 keV aiming to identify potential beam effects. Fig. 7 shows the patterns taken during the pulse for NMC containing blends measured for both energies. The expected peak evolution is observed in both cases, yet a more distinct pattern evolution is seen at 30 keV. Notably, there is a smaller peak intensity variation between the patterns as well as less broadening which could be attributed to a more homogeneous lithiation in the area under irradiation. For both NMC-LMO and NMC-LFMP blends, the $(003)_{NMC}$ peak in Fig. 7 does not reach the expected position at full lithiation at 15 keV. This discrepancy is resolved at 30 keV, where the $(003)_{NMC}$ peak overlaps with the $(111)_{LMO}$ peak. For NMC-LFMP the peak in the final pattern at 15 keV is broader and exhibits lower intensity, in agreement with a less homogeneous lithiation degree in the irradiated area. Once again this is not the case for 30 keV. For NMC-LFP, the $(003)_{NMC}$ peak appears to reach to its final state also at 15 keV, yet this is attributed most likely to LFP being a lower voltage material expected to start lithiating after NMC is fully lithiated. This results in NMC spending a large fraction of the discharge time in the fully lithiated state and as such having more time to reach its final state, which might be perceived as reduced reaction kinetics. Comparing the patterns at different energies, it can be concluded that significant differences occur based on beam photon energy, with higher energy photons proving effective in minimizing beam related effects and this dependence is in line with recently published works [24]. Some of the studied active materials, namely NMC and LFP, were found to be more sensitive to such phenomena. Electrochemistry showed no signs of alteration from the beam, which could be explained with the fact that the illuminated area accounted only for approximately 6 % (~10 mm^2) of the total electrode area (~154 mm^2).

Measuring at higher energy (lower wavelength) comes however with the drawback of the patterns appearing "compressed". This is evident from the x axes scales of Fig. 7, where the same peaks are being pictured for both energies. This effect, paired with the fact that kinetics at 15 keV seem slower despite all precautions taken, increase the possibility that the buffer effect is better captured at 15 keV, potentially enabling us to leverage beam effects to our advantage.

Fig. 8 shows selected pulses where all the patterns obtained for each relaxation (approx. 160 patterns) are depicted evolving from black (immediately after current interruption) to yellow (after 10 min of no current) at 15 keV (same plots for 30 keV are shown in Fig. 5S.I.). For the understanding of the results, one can make predictions using the decoupled blends study. For the case of NMC-LMO, as seen in Fig. 3, during relaxation of pulse 1, lithium is transferred from LMO to NMC which is also witnessed in the diffraction in Fig. 8a where the $(003)_{NMC}$ peak shifts towards lower angles indicating lithiation while $(111)_{LMO}$ peak shifts slightly towards higher angles showing evidence of delithiation. For the relaxation of pulse 4 (Fig. 8b), decoupled blends predict lithiation of LMO and delithiation of NMC yet in diffraction only the lithiation of LMO is witnessed, evidenced by the shift of the $(111)_{LMO}$ peak towards lower angles. Finally, for pulse 16, lithium exchange is expected to happen from LMO to NMC, and once again only the lithiating component was witnessed. Delithiation is also captured for the NMC-LFP through an increase in the intensity of $(002)_{LFP}$ peak. In general, even though delithiation was proven challenging to evidence in XRD, the material that was witnessed relaxing was in the vast majority of cases in line with the decoupled blends experiment and this serves as a direct proof of the buffer effect in the electrodes under study, as predicted by the decoupled blends.

The difficulty in witnessing the delithiation can be rationalized in terms of electrode kinetics. Due to the technical nature of the cell, the area where the windows are experiences a lower stack pressure in addition to being irradiated. Both can contribute in the slower kinetics of the materials, with 15 keV experiments seemingly experiencing a

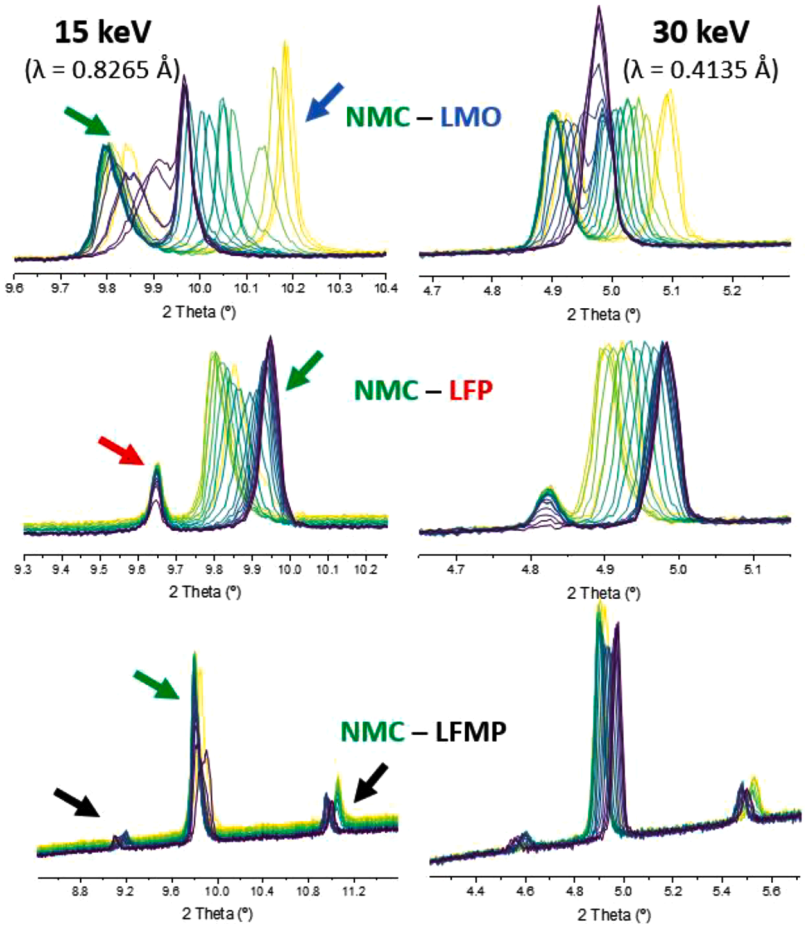

Fig. 7. First pattern recorded for each of the pulses at 15 keV (= 0.8265 Å) and 30 keV (λ = 0.4135 Å). Arrows are colour coded according to the material to which each peak corresponds.

stronger effect. After the pulse, lithiation naturally homogenizes throughout the electrode, and a general influx of lithium is expected from faster kinetically active areas towards the slower ones—specifically, the area under test. This phenomenon is expected to be superimposed to the buffer effect and as such favour the witnessing of the lithiation while potentially masking the delithiation. Nevertheless, delithiation is still expected to occur whenever the buffering effect is stronger and, as discussed above, this has been the case in certain pulses.

3.5. Discussion

Despite blended electrodes being widely used in commercial cells, transition from empiricism to full understanding of the internal dynamics with the aim of being able to predict properties is hampered by the complexity of the system, which is also tricky to capture through modelling [27]. Thus, getting experimental data on a range of blend model systems under controlled operation conditions is crucial to shed light on their operation mechanism and advance towards *ad hoc* rational design of the blends to match specific application demands.

The results achieved within this study illustrate how the performance of blended electrodes, besides depending on the kinetics of each individual component (influenced by both electronic and ionic conductivities, which can also vary with the SoC), is influenced by thermodynamics (voltage profiles). Indeed, these play a role on the extent and directionality of the current/lithium exchanged between components, which exhibit relevant variations throughout the full range of operation. Even if the study does not cover changes in the ratio between the components, it is clear that the blending fraction will have an additional effect on these aspects. Considering a material that takes the whole cell current at a certain voltage, its effective operation rate will be dictated by its fraction. In a hypothetical blend of materials A and B of equal theoretical capacities where A is 20 % of the active mass, if all the cell current is provided by A at a certain voltage, its effective rate would be 5 times higher than the cell's nominal rate. Yet, if it's material B that provides all cell current, its effective rate will be only 1.25 times higher. Thus, it can be expected that using a small fraction of a material with a plateau in a blend would cause it to experience exceedingly high rates when the cell voltage coincides with the one of the plateau.

Since for many materials kinetics are a function of SoC, blending could be used as a strategy to relief or stress operation at certain voltage. During pulsed operation the magnitude of the "buffer effect" in the electrode will be dictated by effective overpotentials on blend component. Since overpotential is not only related to intrinsic properties of materials but also affected by other aspects, such as particle size or electrode related parameters (e.g. porosity and tortuosity), these can provide an additional tool to tune the ability and extent of buffering. Because overpotential will itself be dependent on the SoC, a significant influence of the blending ratio on the buffering can also be expected.

Thermodynamics will dictate the direction of the buffering current which can be deduced from the individual voltage profiles. At a given SoC this direction is expected to be the same upon charge and discharge. Shall buffering occur, a material A with only a high voltage plateau is expected to act as a lithium acceptor during post-pulse relaxation upon discharge when blended with a material B with a lower voltage plateau. Kinetics will only affect the magnitude of the phenomenon, as the overpotential of A grows, it becomes easier to enter the operation voltage range of B and induce the buffer effect. Yet, buffering will no longer be possible once the high voltage material becomes fully

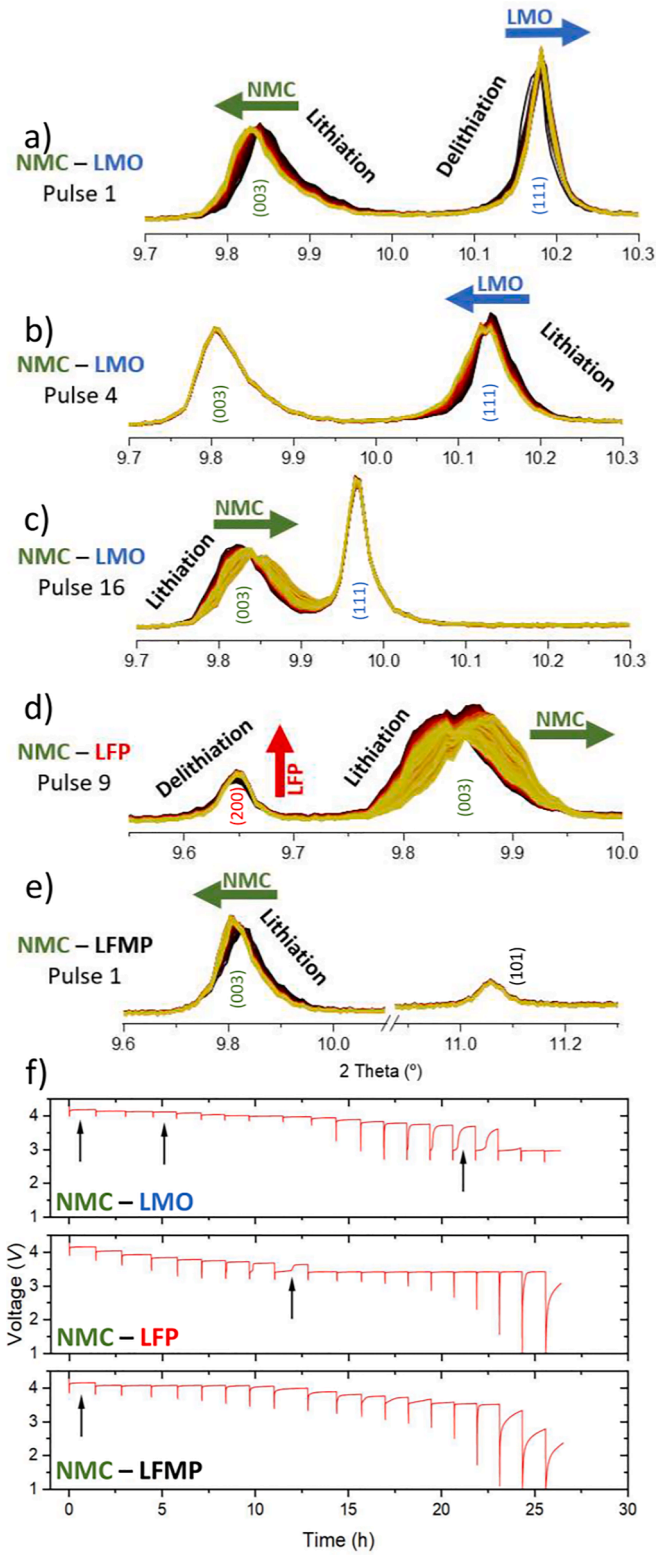

Fig. 8. (a–e) Selected relaxations of measured blends showing peak evolution, black is the first pattern obtained after the pulse and yellow is the last. Arrows are colour coded according to material and act as a guide to the eye for the peak shift observed during relaxation. On top of each peak, the shift observed is linked to the materials (de)lithiation. f) Voltage as a function of time for the blends pictured. The black arrows indicate the relaxations shown in plots a-e.

lithiated. Reversing the current on the same system is expected to reverse the buffering "roles", now, the low voltage component B, due to overpotential, can enter the active regime of the higher voltage material A, enabling material B to be buffered.

Operando XRD measurements have allowed to capture charge transfer events in real blends, providing a deeper understanding of their behavior. However, the challenges associated with time-resolved XRD, particularly potential beam effects, need careful consideration to ensure the reliability and accuracy of the obtained data. Despite these challenges, the results obtained from operando XRD are in good agreement with those of decoupled electrochemical experiments.

In conclusion, the results presented herein showcase the importance of a holistic approach in studying complex electrode systems. Further work should be addressed to extend this studyto a wider set of temperatures, compositions and blend component ratios (eventually considering ternary [28] or even quaternary compositions), the ultimate goal being to achieve predictive understanding and rationalization of blend design to match specific application operation needs.

4. Conclusions

The study of a wide set of binary blend electrodes with a range of different components but keeping a 50:50 ratio between them serves as a valuable complement to previous work carried out on specific blends (e.g. NMC-LMO) with varying compositions. The results presented herein facilitate the assessment of the influence of the voltage profile of the components in the extent and directionality of the charge transfer between them, which is further shown to be dependent on the cell SoC and the operation temperature. The trends deduced from electrochemical experiments carried out using the decoupled blend setup were found to be in very good agreement with those derived from *operando* XRD on real blended electrodes in which the components are in physical contact, which evidences the representativity of this experimental approach. Assessing the influence of thermodynamic factors constitutes an additional step to progress in the mechanistic understanding of blended electrodes, which is obviously greatly influenced by the reaction kinetics of the individual materials (that also depend on SoC). The findings presented in this study offer a foundational framework for the design of blended electrodes customized to specific application requirements and pave the way for a more informed and strategic approach to developing blended electrodes.

CRediT authorship contribution statement

Dimitrios Chatzogiannakis: Writing – original draft, Visualization, Validation, Methodology, Investigation, Formal analysis, Data curation. **Violetta Arszelewska:** Writing – review & editing, Formal analysis. **Pierre-Etienne Cabelguen:** Writing – review & editing, Formal analysis. **François Fauth:** Writing – review & editing, Investigation. **Montse Casas-Cabanas:** Writing – review & editing, Writing – original draft, Supervision, Funding acquisition, Conceptualization. **M. Rosa Palacin:** Writing – review & editing, Writing – original draft, Supervision, Funding acquisition, Conceptualization.

Declaration of competing interest

The authors declare the following financial interests/personal relationships which may be considered as potential competing interests:

M. Rosa Palacin reports financial support was provided by Spanish research agency. M. Rosa Palacin reports financial support was provided by H2020 MSCA COFUND Actions. If there are other authors, they declare that they have no known competing financial interests or personal relationships that could have appeared to influence the work reported in this paper.

Data availability

Data will be made available on request.

Acknowledgements

Authors are grateful for access to ALBA synchrotron for beamtime (proposal 2023027430). ICMAB-CSIC members thank the Spanish Agencia Estatal de Investigación Severo Ochoa Programme for Centres of Excellence in R&D (CEX2019–000917-S) and funding through grant PID2020–113805GB-I00. This work has been done in the framework of the doctorate in Materials Science of the Universitat Autònoma de Barcelona and D.C. acknowledges DESTINY MSCA PhD Programme funded by the European Union's Horizon 2020 research and innovation programme under Grant Agreement No 945357. Authors acknowledge support of the publication fee by the CSIC Open Access Publication Support Initiative through its Unit of Information Resources for Research (URICI).

Supplementary materials

Supplementary material associated with this article can be found, in the online version, at doi:10.1016/j.ensm.2024.103414.

References

[1] R. Schmuch, R. Wagner, G. Hörpel, T. Placke, M. Winter, Performance and cost of materials for lithium-based rechargeable automotive batteries, Nat. Energy 3 (2018) 267–278.
[2] T. Numata, C. Amemiya, T. Kumeuchi, M. Shirakata, M. Yonezawa, Advantages of blending LiNi0.8Co0.2O2 into Li1+xMn2−xO4 cathodes, J. Power Sources 97–98 (2001) 358–360.
[3] S.B. Chikkannanavar, D.M. Bernardi, L. Liu, A review of blended cathode materials for use in Li-ion batteries, J. Power Sources 248 (2014) 91–100.
[4] H.Y. Tran, C. Täubert, M. Wohlfahrt-Mehrens, Influence of the technical process parameters on structural, mechanical and electrochemical properties of LiNi0.8Co0.15Al0.05O2 based electrodes – a review, Prog. Solid State Chem. 42 (2014) 118–127.
[5] A.J. Smith, S.R. Smith, T. Byrne, J.C. Burns, J.R. Dahn, Synergies in blended LiMn2O4 and Li [Ni1/3Mn1/3Co1/3]O2 positive electrodes, J. Electrochem. Soc. 159 (2012) A1696.
[6] H.Y. Tran, et al., LiMn2O4 Spinel/LiNi0.8Co0.15Al0.05O2 blends as cathode materials for lithium-ion batteries, J. Electrochem. Soc. 158 (2011) A556.
[7] N.M. Jobst, A. Hoffmann, A. Klein, S. Zink, M. Wohlfahrt-Mehrens, Ternary cathode blend electrodes for environmentally friendly lithium-ion batteries, ChemSusChem 13 (2020) 3928–3936.
[8] G. Sun, et al., Synergistic effect between LiNi0.5Co0.2Mn0.3O2 and LiFe0.15Mn0.85PO4/C on Rate and Thermal Performance for Lithium Ion Batteries, ACS Appl. Mater. Interfaces 10 (2018) 16458–16466.
[9] D. Westhoff, et al., Analysis of microstructural effects in multi-layer lithium-ion battery cathodes, Mater. Charact. 151 (2019) 166–174.
[10] T. Liebmann, C. Heubner, M. Schneider, A. Michaelis, Understanding kinetic and thermodynamic properties of blended cathode materials for lithium-ion batteries, Mater. Today Energy 22 (2021) 100845.
[11] T. Liebmann, C. Heubner, M. Schneider, A. Michaelis, Investigations on the reversible heat generation rates of blended Li-insertion electrodes, J. Solid State Electrochem. 23 (2019) 245–250.
[12] C. Heubner, M. Schneider, A. Michaelis, Reversible heat generation rates of blended insertion electrodes, J. Solid State Electrochem. 21 (2017) 2109–2115.
[13] C. Heubner, T. Liebmann, C. Lämmel, M. Schneider, A. Michaelis, Internal dynamics of blended Li-insertion electrodes, J. Energy Storage 20 (2018) 101–108.
[14] J. Huang, et al., Entropy coefficient of a blended electrode in a lithium-ion cell, J. Electrochem. Soc. 162 (2015) A2367.
[15] M. Yue, et al., Improved elevated temperature performance of LiFePO4/Graphite cell by blending NMC640 in cathode, J. Electrochem. Soc. 170 (2023) 110532.
[16] C. Heubner, T. Liebmann, M. Schneider, A. Michaelis, Recent insights into the electrochemical behavior of blended lithium insertion cathodes: a review, Electrochim. Acta 269 (2018) 745–760.
[17] M. Casas-Cabanas, A. Ponrouch, M.R. Palacín, Blended positive electrodes for Li-ion batteries: from empiricism to rational design, Isr. J. Chem. 61 (2021) 26–37.
[18] T. Liebmann, C. Heubner, C. Lämmel, M. Schneider, A. Michaelis, Investigations on the effective electric loads in blended insertion electrodes for lithium-ion batteries, ChemElectroChem. 6 (2019) 5728–5734.
[19] C. Heubner, T. Liebmann, C. Lämmel, M. Schneider, A. Michaelis, Deconvolution of cyclic voltammograms for blended lithium insertion compounds by using a model-like blend electrode, ChemElectroChem 5 (2018) 425–428.
[20] D. Chatzogiannakis, et al., Towards understanding the functional mechanism and synergistic effects of LiMn2O4 - LiNi0.5Mn0.3Co0.2O2 blended positive electrodes for Lithium-ion batteries, J. Power Sources 591 (2024) 233804.
[21] M. Herklotz, et al., A novel high-throughput setup for *in situ* powder diffraction on coin cell batteries, J. Appl. Crystallogr. 49 (2016) 340–345.
[22] D. Saurel, et al., Experimental considerations for operando metal-ion battery monitoring using X-ray techniques, Chem. Methods 1 (2021) 249–260.
[23] T. Jousseaume, J.F. Colin, M. Chandesris, S. Lyonnard, S. Tardif, How beam damage can skew synchrotron operando studies of batteries, ACS Energy Lett. 8 (2023) 3323–3329.
[24] C.K. Christensen, et al., Beam damage in operando X-ray diffraction studies of Li-ion batteries, J. Synchrotron. Radiat. 30 (2023) 561–570.
[25] L. Blondeau, et al., Are operando measurements of rechargeable batteries always reliable? An example of beam effect with a Mg battery, Anal. Chem. 94 (2022) 9683–9689.
[26] P. Black, et al., Beam Effects in Synchrotron Radiation Based Operando Characterization of Battery Materials: XRD and XAS Study of LiNi0.33Mn0.33Co0.33O2 and LiFePO4 Electrodes, Submitted for publication, 2024.
[27] C. Heubner, T. Liebmann, C. Lämmel, M. Schneider, A. Michaelis, Synergy effects in blended electrodes for Li-ion batteries: a conceptual clarification, Batter. Supercaps. 5 (2022) e202100171.
[28] M.S.D. Darma, et al., The influence of cycling temperature and cycling rate on the phase specific degradation of a positive electrode in lithium ion batteries: a post mortem analysis, J. Power Sources 327 (2016) 714–725.